ACM SIGGRAPH / Eurographics Symposium on Computer Animation 2020
J. Bender and T. Popa
(Guest Editors)

Volume 39 (2020), Number 8

Primal/Dual Descent Methods for Dynamics

M. Macklin[1,2], K. Erleben[2], M. Müller[1], N. Chentanez[1], S. Jeschke[1], T.Y. Kim[1]

[1]NVIDIA
[2]University of Copenhagen

Abstract

We examine the relationship between primal, or force-based, and dual, or constraint-based formulations of dynamics. Variational frameworks such as Projective Dynamics have proved popular for deformable simulation, however they have not been adopted for contact-rich scenarios such as rigid body simulation. We propose a new preconditioned frictional contact solver that is compatible with existing primal optimization methods, and competitive with complementarity-based approaches. Our relaxed primal model generates improved contact force distributions when compared to dual methods, and has the advantage of being differentiable, making it well-suited for trajectory optimization. We derive both primal and dual methods from a common variational point of view, and present a comprehensive numerical analysis of both methods with respect to conditioning. We demonstrate our method on scenarios including rigid body contact, deformable simulation, and robotic manipulation.

CCS Concepts

• ***Computing methodologies*** → ***Simulation by animation;*** *Interactive simulation;* • ***Computer systems organization*** → *Robotics;*

Keywords: contact, friction, numerical optimization, robotics

1. Introduction

Implicit time integration is popular in computer graphics and robotics for its robustness and efficiency. Given a continuous time dynamics model, an implicit time discretization will generally result in a nonlinear system of equations. Many numerical methods have been proposed to solve these discretized equations of motion, which we categorize broadly as *primal* and *dual* methods. The terms primal and dual are perhaps most appropriate when viewing implicit integration as a *variational* problem that formulates time stepping as an energy minimization. Primal methods we consider as ones that are expressed and solved in terms of the system degrees of freedom, i.e.: positions, velocities, and the forces acting on them. On the other hand, dual methods focus on constraints between the degrees of freedom, and solve in terms of their Lagrange multipliers.

In this work, we show that both primal methods such as Projective Dynamics (PD) [BML*14] and dual methods, such as extended Position-based Dynamics (XPBD) [MMC16], may both be derived from a common variational basis, and offer complementary tradeoffs in terms of sensitivity to poorly conditioned problems. While primal descent methods have been used successfully for elasticity simulation [Wan15, WY16], they have not found wide-spread use in contact-rich scenarios, such as rigid body simulation. We extend these methods to dry frictional contact by deriving a Coulomb friction model from a variational basis, and provide an efficient preconditioner suitable for parallelization. Our primal formulation of contact possesses a number of desirable traits. First, it is differentiable,

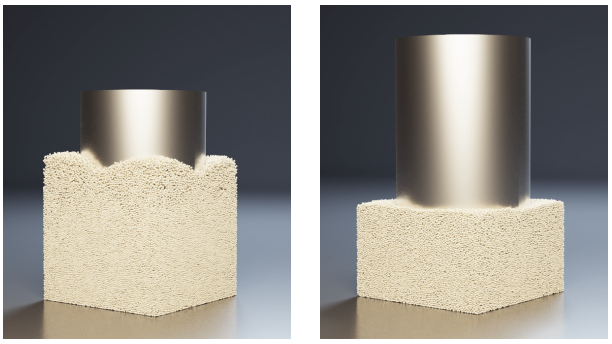

(a) (b)

Figure 1: ***Granular Material****. In this example the granular medium consists of 256k rigid bodies with an average radius of 5mm. The resulting mass ratio between the grains and cylinder is* 80000 : 1*, which results in an ill-conditioned system for dual, or constraint-based solvers (left). Primal formulations on the other hand are relatively unaffected by this ratio (right).*

and has well-defined inverse dynamics, an important property for trajectory optimization [Tod14]. Second, it is insensitive to mass-ratios, allowing it to stably simulate scenarios involving both small and large bodies, as shown in Figure 1. Third, it does not require the tracking of auxiliary variables such as Lagrange multipliers. This means that the system size remains constant over the course of a simulation, which may be desirable if using the system state as an input to e.g.: a neural network controller [PRM19]. Finally, we find that the force distributions obtained from relaxed, or compliant, contact models, are smoother than the result from hard-contact models, this can be desirable when contact forces act as input to control algorithms. In summary, our technical contributions are as follows:

- A derivation of primal and dual formulations of contact dynamics from a common variational basis. Our derivation shows the underlying connection between methods such as Projective Dynamics and XPBD, and extends the Projective Dynamics-based method of [Wan15] to rigid body simulation.
- A primal frictional contact model derived from a variational basis. Our model is simple to implement, supports differentiability, and is well-suited to GPUs.
- A numerical analysis of the sensitivity of both primal and dual descent methods to ill-conditioned problems. We test the relative strengths / weaknesses of each method in the presence of large mass ratios, and identify the lesser known problem of stiffness ratios.
- An experimental comparison of both optimization methods on a number of scenarios including unstructured piling, robotic grasping, cloth simulation, and trajectory optimization.

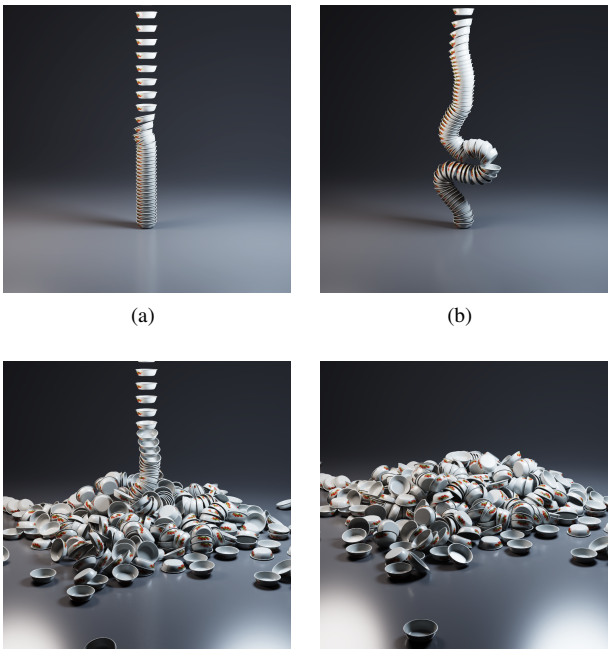

Figure 2: ***Unstructured Piling****. A sequence of frames from a large-scale piling example inspired by Xu & Barbic [XZB14]. Despite having 393k (40x more) contacts, our parallel preconditioned gradient descent solver runs at real time rates.*

2. Related Work

We now discuss some previous simulation work in both the primal and dual space with a focus on elasticity and contact simulation.

2.1. Elasticity

There has been a large amount of work on implicit simulation of elastic bodies in computer graphics. Baraff & Witkin [BW98] proposed a single-step Newton method for solving the discrete implicit equations of motion in cloth simulation. They use a linearization of forces that results in significant artificial damping, and has led to the development of a number of nonlinear implicit solvers. Many of these are derived from variational principles, which formulate the problem as one of energy minimization [GSS*15, MKB*10]. In particular, Projective Dynamics (PD) [BML*14, LBOK13], proposes a splitting-based method where elastic potentials are handled through a local projection, and inertial potentials that are handled through a global step. Wang et al. [Wan15, WY16] showed that descent methods applied to variational implicit Euler may be considered as a special case of Projective Dynamics where the local and global solve are performed using one preconditioned Jacobi iteration. In this work we also focus on preconditioned descent methods for their simplicity and simple GPU parallelization. We extend the work of Wang et al. to include rigid bodies, and a contact model based on a variational energy function that correctly models Coulomb friction.

Constraint-based, or dual methods are also popular for elastic and multi-body dynamics. Servin et al. [SLM06] formulated a linear finite element method (FEM) as a set of compliant constraints. This approach was made robust by the inclusion of geometric stiffness terms that include second order constraint information [TNGF15, ATK17]. Goldenthal et al. [GHF*07] proposed a fast constraint projection method using direct solvers, while Position-based Dynamics employs iterative, local, nonlinear constraint projections on the same constraint-based formulation [MHHR07, Sta09]. This approach was extended to correctly handle quadratic energy potentials in XPBD [MMC16], and we show how these methods may be seen as solving a dual variational problem, which we derive in Section 3.3.

2.2. Contact

Penalty methods are a common primal model of contact in graphics and robotics [MO96, YN06, Dru07, TMOT12]. While explicit penalty methods tend to require small time-steps for stability, the combination of implicit penalty contact with direct solvers has been successfully employed [XZB14]. A notable example is in MuJuCo [TET12, Tod14], which uses a relaxed contact model inside an acceleration-based framework with direct solver methods. We present a primal contact model inspired by this work and combine it

with a descent-based solver well-suited for GPU implementations and capable of scaling to hundreds of thousands of simultaneous contacts. While relaxed methods of contact generally permit some interpenetration or slip, we find this is not a significant limitation, as illustrated in Figure 3.

Pan et al. [PRM19] used a smooth contact model for differentiable trajectory optimization. They propose a viscous friction model that, does not make a distinction between stick and slip regimes. In this work we propose a relaxed friction model that also captures the Coulomb constraint that friction forces should lie inside the friction cone. Hybrid methods for contact have also been used successfully. An example of this is the work by Tang et al. [TWL*18], who used the augmented Lagrangian method (ALM) to resolve cloth self-collisions. Kaufman et al. [KSJP08] proposed staggered projections for frictional contact where interpenetration is prevented through interleaved quadratic programming (QP) solves. Their resulting optimization problem may be solved using primal or dual methods. Mazhar et al. [MMFN14] compared primal and dual formulations of contact modeled as hard constraints and their effect on solution methods.

Simultaneous to our work, Li et al. [LFS*20] proposed a lagged primal formulation of contact that uses barrier methods to guarantee interpenetration free states. While barrier methods prevent touching contact, we focus on implicit penalty methods, which permit some interpenetration. We propose a similar smoothed friction model derived from a variational dissipation potential and compare primal and dual methods for solving the resulting optimization problem. Recent work has extended Projective Dynamics to handle nodal frictional contact for cloth and thin objects [LJBBD20, Dav20]. Since our method is based on the descent-based Projective Dynamics solver of [WY16] it is not limited to nodal contact, and may also be used for rigid bodies. Brown et al. [BOFN18] also presented a non-smooth dissipation potential to model friction in the Projective Dynamics framework. We present a smooth extension of this model that has continuous derivatives.

In the dual space, Stewart & Trinkle [ST96] proposed an implicit time-stepping scheme for rigid body contact using a linear complementarity (LCP) formulation. This model has become popular in graphics, especially when combined with iterative LCP solvers such as projected Gauss-Seidel (PGS) and projected Jacobi [OTSG09, DBDB11, Erl13, BET14, NE15, TBV12, VJ19]. Dual formulations of contact naturally handle hard contact and static friction constraints. On the other hand, hard models of contact may become overdetermined through incompatible contact constraints, for example a body being squeezed between two immovable objects. In this case numerical methods may return an arbitrary answer, or in the case of direct methods may fail to produce any answer at all. Hard contact problems may also become underdetermined, for example a tessellated cylinder resting on the ground with multiple contact points. In this case there exist many possible solutions, and the result will typically depend on the constraint order given to the solver. In contrast, our relaxed primal model of contact generates well-posed problems that result in smooth contact force distributions as we demonstrate in Figure 11.

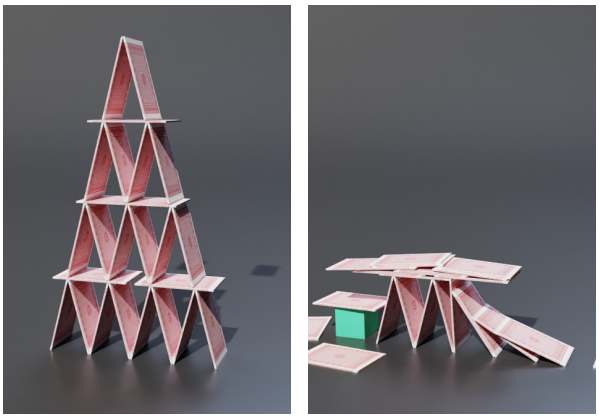

Figure 3: ***Structured Stacking****. A classic stacking test involving a house of cards. We find that, until knocked down by an external body, implicit primal contact is able to achieve similarly stable structures to traditional dual methods.*

3. Optimization-based Time Integration

In this section we introduce our implicit time-stepping scheme. We show how this may be formulated as a discrete variational optimization problem, and solved by either primal or dual numerical methods. We analyze the sensitivity and relative strengths of both methods in Section 4.

To begin, we define the generalized system coordinates and their time derivatives as $\mathbf{q}$ and $\dot{\mathbf{q}}$ respectively. To simplify the following derivations we re-parameterize the system by introducing the discrete velocity $\mathbf{u}^+$, and the relationship $\mathbf{q}^+ = \mathbf{q}^- + h\mathbf{G}\mathbf{u}^+$, where the superscripts $+/-$ are shorthand to indicate the state at t and $t+\Delta t$, i.e.: the beginning and end of the time-step, respectively. The matrix $\mathbf{G}$ is a *kinematic map* that maps spatial velocities to system coordinate time derivatives, i.e.: $\dot{\mathbf{q}} = \mathbf{G}\mathbf{u}$ [BET14]. This velocity re-parameterization allows us to treat rigid bodies and particles in a unified manner. Our discrete equations of motion are then

$$\mathbf{M}\left(\mathbf{u}^+ - \tilde{\mathbf{u}}\right) - \Delta t \mathbf{f}(\mathbf{q}^+, \mathbf{u}^+) = \mathbf{0}. \tag{1}$$

Where the constant $\tilde{\mathbf{u}} \equiv \mathbf{u}^- + \Delta t\, \mathbf{M}^{-1}\left(\mathbf{f}_{\text{ext}} + \mathbf{f}_{\text{gyro}}\right)$ is the unconstrained velocity that includes the external and gyroscopic forces integrated explicitly. As shown in previous works, implicit time integration can be formulated as an optimization problem [BBB07, BML*14, GSS*15]. First, we define the objective function:

$$g(\mathbf{u}) \equiv \frac{1}{2}\left(\mathbf{u} - \tilde{\mathbf{u}}\right)^T \mathbf{M}\left(\mathbf{u} - \tilde{\mathbf{u}}\right) + \sum_i U_i\left(\mathbf{q}^+(\mathbf{u})\right), \tag{2}$$

where U_i are arbitrary energy potentials that give rise to the forces $\mathbf{f}$ on the system. The optimization problem is then,

$$\mathbf{u}^+ \equiv \underset{\mathbf{u}}{\operatorname{argmin}}\, g(\mathbf{u}). \tag{3}$$

The benefit of stating implicit time integration in this variational form is that many robust methods exist to solve such optimization problems, allowing a more unified treatment. We are primarily interested in first order methods, i.e.: those that use only information about the gradient of g since they are simple to implement, and well suited for parallelization [WY16]. In the following section we will show how to use second order information when available. Note that the gradient of the objective (2) is simply given by (1), i.e.:

$$\mathbf{d}\big|_{\mathbf{u}^+} \equiv \frac{\partial g}{\partial \mathbf{u}}^T\Bigg|_{\mathbf{u}^+} = \mathbf{M}\left(\mathbf{u}^+ - \tilde{\mathbf{u}}\right) - \Delta t \mathbf{f}(\mathbf{q}^+, \mathbf{u}^+) \tag{4}$$

where the generalized force is $\mathbf{f} = -\sum_i \mathbf{G}^T \frac{\partial U_i^T}{\partial \mathbf{q}^+}$.

3.1. Gradient Descent

Perhaps the simplest approach to solving the minimization (3) is gradient descent. In this scheme we repeatedly update the solution $\mathbf{u}^+$ and $\mathbf{q}^+$ as follows:

$$\mathbf{u}^+ \leftarrow \mathbf{u}^+ - \alpha \mathbf{d} \tag{5}$$

$$\mathbf{q}^+ \leftarrow \mathbf{q}^- + \Delta t \mathbf{G}\mathbf{u}^+ \tag{6}$$

where α is a step-length parameter. In practice gradient descent converges very slowly and a line search is necessary to avoid overshooting and divergence. We can improve the convergence of gradient descent by defining a preconditioning matrix $\mathbf{P}$. Provided an appropriate choice of $\mathbf{P}$ such that $\mathbf{d}^T \mathbf{P}\mathbf{d} > 0$, our descent update for $\mathbf{u}^+$ is then

$$\mathbf{u}^+ \leftarrow \mathbf{u}^+ - \alpha \mathbf{P}\mathbf{d}. \tag{7}$$

A common choice for $\mathbf{P}$ is the Hessian inverse, i.e.: $\mathbf{P} \approx \mathbf{H}^{-1} \equiv \frac{\partial^2 g}{\partial \mathbf{u}^2}^{-1}$, which corresponds to Newton's method. Due to potential indefiniteness and the complexity of evaluating the Hessian many approaches exist to approximate $\mathbf{P}$ leading to a range of quasi-Newton methods. In the following section we review and compare some common choices and discuss their relationship.

3.2. Quadratic Potentials

The primal descent method presented above is applicable to any nonlinear conservative force. However, to draw comparisons to other methods we first consider the special case of quadratic energy potentials. Consider a single potential of the form,

$$U \equiv \frac{1}{2} k C(\mathbf{q})^2, \tag{8}$$

where k is a stiffness parameter, and $C(\mathbf{q})$ a constraint function that can be either a scalar or vector function. We define the corresponding generalized force arising from U as,

$$\mathbf{f} = -\mathbf{G}^T \frac{\partial U}{\partial \mathbf{q}}^T = -k \mathbf{J}^T C(\mathbf{q}), \tag{9}$$

where the constraint Jacobian is given by $\mathbf{J} = \frac{\partial C}{\partial \mathbf{q}}\mathbf{G}$. For a Newton style preconditioner we need the Hessian, $\mathbf{H}$, of our objective function g with respect to the solution variable $\mathbf{u}$,

$$\mathbf{H} \equiv \frac{\partial^2 g}{\partial \mathbf{u}^2} = \mathbf{M} - \Delta t \frac{\partial \mathbf{f}}{\partial \mathbf{u}}. \tag{10}$$

Assuming the mass $\mathbf{M}$ is known, the term to be computed is the force Jacobian $\frac{\partial \mathbf{f}}{\partial \mathbf{u}}$, which, for a quadratic potential, is given by,

$$\frac{\partial \mathbf{f}}{\partial \mathbf{u}} = -\Delta t k \left[\mathbf{J}^T \mathbf{J} + \frac{\partial \mathbf{J}}{\partial \mathbf{u}} C\right]. \tag{11}$$

Here, the second term corresponds to geometric stiffness [TNGF15, ATK17]. Using just first-order terms, the preconditioner is

$$\mathbf{P}^{GN} \equiv \left[\mathbf{M} + \Delta t^2 k \mathbf{J}^T \mathbf{J}\right]^{-1} \approx \left[\frac{\partial^2 g}{\partial \mathbf{u}^2}\right]^{-1}, \tag{12}$$

which corresponds to a Gauss-Newton iteration on g. To avoid computing the inverse, or solving a system of equations, we use a simple diagonal approximation, where each entry is the reciprocal of the diagonal of $\mathbf{P}^{GN}$, i.e.:

$$\mathbf{P}^D_{dd} \equiv \frac{1}{\mathbf{M}_{dd} + \Delta t^2 k \mathbf{J}_d^2}. \tag{13}$$

Note that d is the index of the degree of freedom, not the constraint. In Section 5 we show how to extend preconditioners of this form to contact and friction.

3.3. Dual Ascent

Given an optimization problem in the form of (3) it is possible to construct a *dual* optimization problem over Lagrange multipliers. In this section we derive the dual problem for the case of quadratic potentials, and show how it leads naturally to constrained dynamics methods such as extended position-based dynamics (XPBD).

To construct the dual of our primal optimization problem we introduce the auxiliary variables $\lambda \equiv -\mathbf{K}\mathbf{c}$ where $\mathbf{K} \equiv \mathrm{diag}[k_1, \ldots, k_n]$ is a matrix of stiffness values, and $\mathbf{c} \equiv [C_1, \ldots, C_n]$ is a vector of constraint functions. This allows us to write the system potential energy as $U \equiv -\frac{1}{2}\mathbf{c}^T\lambda$, and define the following Lagrangian,

$$\mathcal{L}(\mathbf{u}, \lambda) \equiv \frac{1}{2}(\mathbf{u} - \tilde{\mathbf{u}})^T \mathbf{M}(\mathbf{u} - \tilde{\mathbf{u}}) - \lambda^T \mathbf{c}(\mathbf{q}^+) - \frac{1}{2}\lambda^T \mathbf{K}^{-1}\lambda. \tag{14}$$

It can be verified that the stationarity conditions for this Lagrangian correspond to the original problem (3) with quadratic potentials [BV04]. While both primal and dual optimization can be applied to arbitrary energy potentials, the dual formulation requires finding a splitting into Lagrange multipliers that is not always as straightforward as the case for quadratic potentials.

The corresponding Lagrange dual function for (14) is

$h(\lambda) \equiv \inf_{\mathbf{u}} \mathcal{L}(\mathbf{u},\lambda) = \mathcal{L}(\mathbf{u}^*,\lambda)$. In general, the constraint functions are nonlinear, and so we cannot obtain a closed form expression for $\mathbf{u}^*$ in terms of λ. However, assuming constraint linearity we can make the following approximation $\mathbf{u}^* \approx \tilde{\mathbf{u}} + \Delta t \mathbf{M}^{-1}\mathbf{J}^T\lambda$. Inserting this into the Lagrangian, the dual function is then

$$h(\lambda) \approx \frac{\Delta t^2}{2}\lambda^T\left(\mathbf{J}\mathbf{M}^{-1}\mathbf{J}^T\right)\lambda - \lambda^T\mathbf{c}(\mathbf{q}^+) - \frac{1}{2}\lambda^T\mathbf{K}^{-1}\lambda, \tag{15}$$

with a corresponding dual *maximization* problem

$$\lambda^+ \equiv \underset{\lambda}{\operatorname{argmax}}\, h(\lambda). \tag{16}$$

To derive the optimality conditions for (16) we take the derivative of h, keeping in mind that $\mathbf{q}^+$ is implicitly a function of $\mathbf{u}^*$ and in turn λ, to obtain

$$\frac{\partial h}{\partial \lambda} \equiv -\left[\mathbf{c}(\mathbf{q}^+) + \mathbf{K}^{-1}\lambda\right] = \mathbf{0}. \tag{17}$$

This set of nonlinear equations corresponds to the form in the XPBD algorithm [MMC16]. To build a preconditioner we evaluate the Hessian with respect to λ, again differentiating through the definition of $\mathbf{q}^+$, giving:

$$\frac{\partial^2 h}{\partial \lambda^2} \equiv -\left[\Delta t^2\mathbf{J}\mathbf{M}^{-1}\mathbf{J}^T + \mathbf{K}^{-1}\right], \tag{18}$$

which, in the case of a diagonal approximation, the preconditioner for the dual ascent is then

$$\mathbf{P}^D_{ii} = \frac{1}{\Delta t^2\mathbf{J}_i\mathbf{M}^{-1}\mathbf{J}_i^T + \mathbf{K}_{ii}^{-1}}. \tag{19}$$

Note that for maximization the sign of the preconditioner is reversed to ensure an ascent direction. The update step is then

$$\lambda^+ \leftarrow \Pi\left(\lambda^+ + \alpha\mathbf{P}\frac{\partial h}{\partial \lambda}\right), \tag{20}$$

where Π is a projection operator used to enforce bound and friction constraints on the dual variables. This is followed by an update of the primal variables,

$$\mathbf{u}^+ \leftarrow \tilde{\mathbf{u}} + \Delta t\mathbf{M}^{-1}\mathbf{J}^T\lambda^+ \tag{21}$$

$$\mathbf{q}^+ \leftarrow \mathbf{q}^- + \Delta t\mathbf{G}\mathbf{u}^+. \tag{22}$$

This derivation shows how we may obtain dual-space algorithms such as XPBD from the starting point of a primal optimization problem. When using a diagonal preconditioner, the above update for λ^+ is identical to that of a Jacobi XPBD iteration. However, in (21)-(22) the primal variable update differs from XPBD by applying updates from the initial state $\mathbf{q}^-, \mathbf{u}^-$ rather than the current descent iterate. A similar observation was made by Daviet [Dav20]. While this modification ensures the method converges to the same solution as the primal form, we found using the *Fast Projection* update of XPBD where position modifications are applied incrementally was more robust [GHF*07]. We outline both primal and dual methods in Listings (1-2).

(a) Primal (b) Dual

Figure 4: ***Stiffness Ratio Test****. We simulate an elastic double pendulum where the lower spring is 10^4 times stiffer than the upper one. Both springs are stiff enough to easily support the attached weights, however the high stiffness ratio causes ill-conditioning for primal formulations and leads to significant error (stretching). In contrast, dual formulations are insensitive to stiffness ratios, and show the correct behavior.*

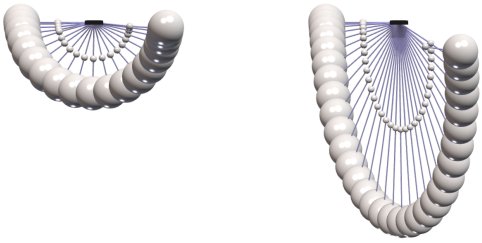

(a) Primal (b) Dual

Figure 5: ***Mass Ratio Test****. A double pendulum consisting of two spheres with a mass ratio of 10^4. High mass ratios cause ill-conditioning for dual methods, which manifests as excessive stretching when using fixed iteration counts. Primal formulations are insensitive to mass ratios and show the correct behavior.*

4. Conditioning

Regardless of the preconditioner used for our numerical method, we can analyze the conditioning of both the primal and dual problems by inspecting their Hessian side-by-side:

$$\frac{\partial^2 g}{\partial \mathbf{u}^2} \equiv \left[\mathbf{M} + \Delta t^2\mathbf{J}^T\mathbf{K}\mathbf{J}\right] \tag{23}$$

$$\frac{\partial^2 h}{\partial \lambda^2} \equiv \left[\Delta t^2\mathbf{J}\mathbf{M}^{-1}\mathbf{J}^T + \mathbf{K}^{-1}\right]. \tag{24}$$

Inspecting the first (primal) case, when $\mathbf{K}$ has a large norm and is

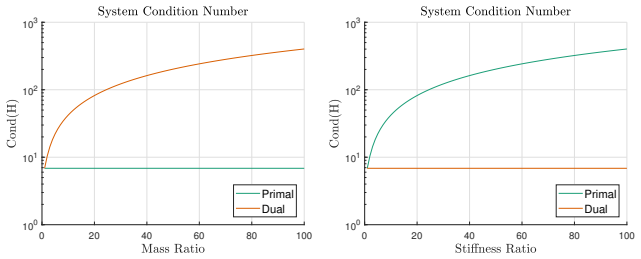

(a) (b)

Figure 6: ***Conditioning****. A plot of the system condition number for a 1D chain of particles with a large mass attached, as shown in Figure 5. As the mass of the weight is increased the condition number of the dual system increases (left). The situation is exactly reversed for the case of stiffness ratios shown in Figure 4, where increasing stiffness leads to poor conditioning (right).*

ALGORITHM 1: Primal Descent Simulation Loop.

while *Simulating* **do**
  Perform collision detection;
  $\mathbf{u}^+ \leftarrow \tilde{\mathbf{u}}$;
  $\mathbf{q}^+ \leftarrow \mathbf{q}^- + \Delta t \mathbf{G}\mathbf{u}^+$;
  for *n descent iterations* **do**
    Initialize force $\mathbf{f}$, and Jacobian diagonal $\mathbf{p}$;
    $\mathbf{f} \leftarrow \mathbf{0}$;
    $\mathbf{p} \leftarrow \mathbf{0}$;
    Evaluate forces and derivatives;
    for *i forces* **do**
      $\mathbf{f} \leftarrow \mathbf{f} + \mathbf{f}_i$;
      $\mathbf{p} \leftarrow \mathbf{p} + \text{diag}\left(\Delta t k_i \mathbf{J}_i^T \mathbf{J}_i\right)$;
    end
    Build preconditioner;
    for *d degrees of freedom* **do**
      $\mathbf{P}^D_{dd} = (\mathbf{M}_{dd} + \Delta t \mathbf{p}_d)^{-1}$;
    end
    Compute gradient;
    $\mathbf{d} \leftarrow \mathbf{M}(\mathbf{u}^+ - \tilde{\mathbf{u}}) - \Delta t \mathbf{f}$;
    Update state;
    $\mathbf{u}^+ \leftarrow \mathbf{u}^+ - \alpha \mathbf{P}^D \mathbf{d}$;
    $\mathbf{q}^+ \leftarrow \mathbf{q}^- + \Delta t \mathbf{G}\mathbf{u}^+$;
  end
end

poorly conditioned (e.g.: there are high stiffness ratios), then this will dominate the mass term and primal descent methods will converge slowly, leading to error, as illustrated in Figure 4. The situation is reversed for the dual form, when $\mathbf{M}$ has a large relative norm and is poorly conditioned (e.g.: high mass ratios) then the system will be hard to solve for iterative dual methods as shown in Figure 5. In Figure 6 we see how, for a simple 1D chain, the condition number of the systems exactly mirror each other for mass/stiffness ratios in each form. While common wisdom states that high stiffness values lead to poorly conditioned systems, this analysis shows that it is actually the *stiffness ratio* that is problematic rather than the absolute stiffness values. We further analyze the effect of this on iterative methods in Section 7.

ALGORITHM 2: Dual Ascent Simulation Loop

while *Simulating* **do**
  Perform collision detection;
  $\mathbf{u}^+ \leftarrow \tilde{\mathbf{u}}$;
  $\mathbf{q}^+ \leftarrow \mathbf{q}^- + \Delta t \mathbf{G}\mathbf{u}^+$;
  for *n ascent iterations* **do**
    Initialize Lagrange multipliers λ, and dual gradient $\mathbf{h}$;
    $\lambda \leftarrow \mathbf{0}$;
    $\mathbf{h} \leftarrow \mathbf{0}$;
    Evaluate constraints and derivatives;
    for *i constraints* **do**
      $\mathbf{h}_i = -C_i(\mathbf{q}^+) - k_i^{-1}\lambda_i$;
      $\mathbf{P}^D_{ii} = \left(\Delta t^2 \mathbf{J_i} \mathbf{M}^{-1} \mathbf{J_i}^T + \mathbf{K}_{ii}^{-1}\right)^{-1}$;
    end
    Compute dual update;
    $\lambda \leftarrow \Pi\left(\lambda + \alpha \mathbf{P}^D \mathbf{h}\right)$;
    Update state;
    $\mathbf{u}^+ \leftarrow \mathbf{u}^+ + \Delta t \mathbf{M}^{-1} \mathbf{J}^T \Delta\lambda$;
    $\mathbf{q}^+ \leftarrow \mathbf{q}^- + \Delta t \mathbf{G}\mathbf{u}^+$;
  end
end

5. Contact

In this section we present a novel primal contact model that incorporates slip and stick regions with a robust preconditioner suitable for implicit integration with descent-based solvers. We first define non-interpenetration constraints using inequalities as follows:

$$C_n(\mathbf{q}) \equiv \mathbf{n}^T \left[\mathbf{a}(\mathbf{q}) - \mathbf{b}(\mathbf{q})\right] - d \geq 0, \tag{25}$$

where $\mathbf{n} \in \mathbb{R}^3$ is the contact plane normal given by the direction vector between closest points of triangle-mesh features, and d is a separation distance to maintain that may be used to model surface thickness. The points $\mathbf{a}$ and $\mathbf{b} \in \mathbb{R}^3$ may be functions of a rigid body frame, or particle positions, in the case of a deformable body. Although we treat the contact normal as fixed over the course of the time step, it is also possible to use a nonlinear constraint on the object motion [LFS*20].

5.1. Complementarity Form

A complementarity formulation of contact enforces the non-penetration condition, 25, as well as the associated Signorini-Fischera condition,

$$0 \leq C_n(\mathbf{q}) \perp \lambda_n \geq 0. \tag{26}$$

The contact force is given by $\mathbf{f}_n(\mathbf{q}) \equiv \mathbf{J}_n^T \lambda_n$, where $\mathbf{J}_n = \frac{\partial C_n}{\partial \mathbf{q}} \mathbf{G}$ is the constraint Jacobian. For iterative dual optimization methods, satisfying the bound constraint on the Lagrange multipliers may be achieved by a simple projection to $\mathbb{R}^+$ which we denote by $\Pi(\lambda_n)$.

5.2. Penalty Form

Penalty methods of contact associate a stiff potential with the contact constraint (25). One view of penalty forms of contact is as a regularization of the complementarity form [Ste00]. In the simplest case this is a function of the clamped constraint error,

$$U_n(\mathbf{q}) \equiv \frac{k_n}{p}\min(0, C_n(\mathbf{q}))^p. \tag{27}$$

where p is a constant exponent (often chosen to be 2). The associated (non-smooth) force due to this potential:

$$\mathbf{f}_n(\mathbf{q}) \equiv -k_n \mathbf{J}_n^T \min(0, C_n(\mathbf{q}))^{p\text{-}1} \tag{28}$$

where k_n controls the stiffness of the contact. One advantage of penalty based approaches is that they can easily support nonlinear contact models [Joh85]. In addition, by varying p we can obtain smoother contact forces that provide continuous derivatives. As shown in Figure 7, when $k_n \to \infty$ the force approaches a hard constraint limit, and as p increases, so does the smoothness of contact forces. To construct a preconditioner for the contact normal force we use the following Hessian approximation:

$$\frac{\partial \mathbf{f}_n}{\partial \mathbf{u}} \approx -\begin{cases} k_n \mathbf{J}_n^T \mathbf{J}_n (p\text{-}1)\min(0, C_n(\mathbf{q}))^{p\text{-}2} & C_n(\mathbf{q}) < 0 \\ \mathbf{0}, & \text{otherwise,} \end{cases} \tag{29}$$

where we have dropped higher order terms corresponding to the geometric stiffness [TNGF15]. This ensures the preconditioner remains positive definite and that the step is in a descent direction. This approximation is justified since, unlike single-step Newton schemes, we repeatedly re-evaluate the constraint gradients throughout the nonlinear solve.

6. Friction

To introduce friction forces we first define the slip velocity at a contact as $\mathbf{u}_s = \mathbf{D}^T\mathbf{u} \in \mathbb{R}^2$, where $\mathbf{D} \in \mathbb{R}^{n\times 2}$ is a basis that projects the bodys' relative velocity to the tangent plane, defined by two orthogonal vectors, perpendicular to the normal $\mathbf{n}$.

6.1. Complementarity Form

Coulomb's friction law may be derived from a principle of maximal dissipation [Ste00] that results in the following conditions on the equations of motion,

$$\mathbf{D}^T\mathbf{u} + \lambda_s \nabla\psi(\lambda_f) = \mathbf{0} \tag{30}$$

$$0 \le \lambda_s \quad \perp \quad \mu\lambda_n - \psi(\lambda_f) \ge 0. \tag{31}$$

Here $\lambda_f \in \mathbb{R}^2$ is a vector of frictional Lagrange multipliers, λ_s is a slack variable that controls stick/slip transitions, $\psi(\lambda_f)$ is a function that encodes the friction cone as a level set, and μ is the coefficient of friction, with the final frictional force given by $\mathbf{f}_f = \mathbf{D}\lambda_f$. As in the contact constraint case, for a descent-based dual solver the complementarity constraints may be enforced by projecting the Lagrange multipliers onto the normal cone [Erl17].

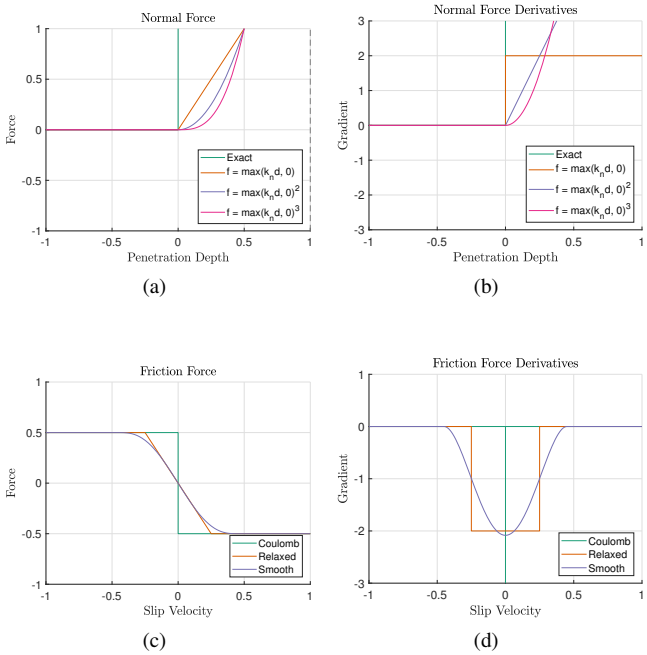

Figure 7: ***Contact Forces****. Relaxed contact models approximate hard contact by replacing the step function with a linear hinge (top left). By exponentiating this function we can obtain C^1/C^2 continuity, with analytic derivatives (top right). Coulomb friction may also be relaxed to obtain invertible contact models (bottom left). The relaxed friction model may then be smoothed to obtain second order differentiability (bottom right).*

6.2. Penalty Form

We now present our novel primal formulation of frictional contact. We postulate a variational energy giving rise to frictional dissipation forces similar to Pandolfi & Ortiz [PO07]. However, to address the issue of indeterminancy in static $\mathbf{u}_s = \mathbf{0}$ case we relax the Coulomb model to include a stiff quadratic region around the origin,

$$U_f(\mathbf{u}) \equiv \begin{cases} \frac{1}{2}k_f|\mathbf{u}_s|^2 & k_f|\mathbf{u}_s| < \mu|\mathbf{f}_n| \\ \mu|\mathbf{f}_n||\mathbf{u}_s| - \gamma, & \text{otherwise.} \end{cases} \tag{32}$$

Here the parameter k_f controls stiffness in the 'stick' regime, where the Coulomb condition $k_f|\mathbf{u}_s| < \mu|\mathbf{f}_n|$ requires that the friction force lie inside the normal cone. We treat $\mathbf{f}_n$ as a constant parameter to the potential, which in the discrete setting corresponds to staggering, or lagging the update of normal forces in the friction calculations between iterations [KSJP08]. The constant $\gamma = \frac{\mu^2|\mathbf{f}_n|^2}{2k_f}$ is chosen to make the potential have C^0 continuity when $k_f|\mathbf{u}_s| = \mu|\mathbf{f}_n|$. This potential is quadratic around the origin and is linear past a certain point (in the slip regime). It gives rise to the following forces:

$$\mathbf{f}_f(\mathbf{u}) \equiv -\min\left(k_f, \mu\frac{|\mathbf{f}_n|}{|\mathbf{u}_s|}\right)\mathbf{D}^T\mathbf{u}_s, \tag{33}$$

which in 1D looks like the relaxed step function as illustrated in Figure 7. To construct a preconditioner for this frictional force we require the potential Hessian, which has the form,

$$\frac{\partial \mathbf{f}_f}{\partial \mathbf{u}} \equiv -\mathbf{D}^T\Lambda\mathbf{D}, \tag{34}$$

with Λ given by

$$\Lambda \equiv \begin{cases} k_f\mathbf{I} & k_f|\mathbf{u}_s| < \mu|\mathbf{f}_n| \\ \mu\frac{|\mathbf{f}_n|}{|\mathbf{u}_s|}\left(\mathbf{I} - \frac{\mathbf{u}_s\mathbf{u}_s^T}{|\mathbf{u}_s|^2}\right) & \text{otherwise.} \end{cases} \tag{35}$$

The term $\mathbf{I} - \frac{\mathbf{u}_s\mathbf{u}_s^T}{|\mathbf{u}_s|^2}$ comes from the derivative of a normalized vector, and accounts for the turning of constraint directions. We found this term can cause gradient descent to fail to converge reliably. Instead we use the simpler, and slightly more conservative scalar Hessian approximation:

$$\Lambda \approx \begin{cases} k_f & k_f|\mathbf{u}_s| < \mu|\mathbf{f}_n| \\ \mu\frac{|\mathbf{f}_n|}{|\mathbf{u}_s|}, & \text{otherwise.} \end{cases} \tag{36}$$

Similar to non-penetration constraints, relaxed friction models may also be smoothed to provide continuous derivatives. This is illustrated in Figure 7, where the quadratic no-slip region in our friction potential is replaced with a 5th degree interpolating polynomial [EMP*03]. Alternatively functions such as the pseudo-Huber norm with higher order continuity exist and may also serve as a smooth friction approximation [CBFAB97].

7. Results

To evaluate our method we implement both primal (corresponding to Projective Dynamics) and dual (corresponding to XPBD) gradient-based optimization methods in CUDA and run them on an NVIDIA Geforce 2080 Ti. For collision detection we use triangle-mesh based contact generation between point-face and edge-edge feature pairs in proximity at start of each time-step. We use a per-frame time step of 16.6 milliseconds (60hz), with a varying number of substeps depending on the example. For rigid body simulation we use a block-diagonal mass matrix, which we invert block-wise to obtain the preconditioner. We use a collision thickness $d \in [10^{-3}, 10^{-2}]$m. As our focus is on real-time applications we use a fixed number of iterations per-time step as reported in Table 1. Line search may be necessary to make gradient-based methods robust. However, for the primal descent method we found that using a fixed value of $\alpha = 0.5$ was sufficient to ensure convergence for all cases we tested. We found dual ascent to be more sensitive to the choice of step length, especially when many contacts influence a single body. To avoid instability in the dual case we have used the mass-splitting approach of Tonge et al [TBV12]. This amounts to treating α as a diagonal matrix that provides a varying step size for each dual variable.

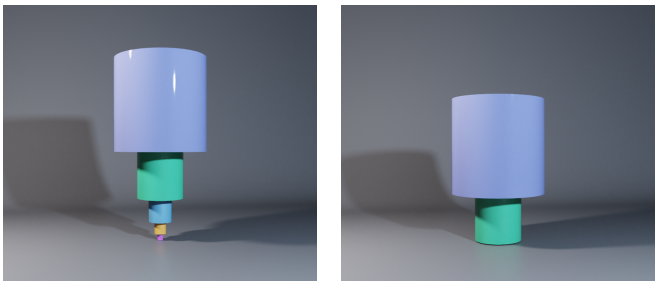

(a) Primal (b) Dual

Figure 8: ***Contact Mass Ratio****. A contact stacking scenario with a mass ratio of 4096:1. Primal solvers are insensitive to this ratio and stack stably in 20 iterations. Conversely, this scenario leads to ill-conditioning for dual methods which fail to stack with 500 iterations.*

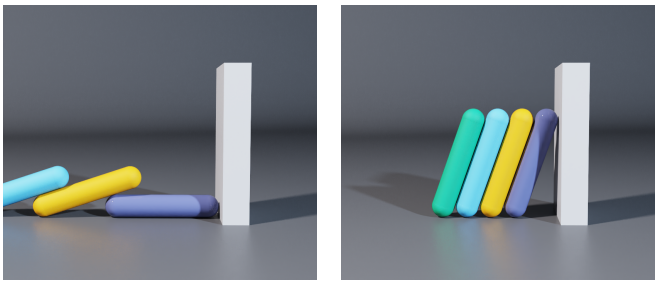

(a) Primal (b) Dual

Figure 9: ***Contact Stiffness Ratio****. An example of a high stiffness ratio contact scenario. In this case we have chosen contact stiffness coefficients of $k_n = 10^8$, and $k_f = 10^6$ creating a stiffness ratio of 100:1. This leads to an ill-conditioned system for primal descent solvers, and results in an inaccurate solution for frictional forces.*

7.1. Mass Ratio Tests

We demonstrate the sensitivity of both primal and dual methods to mass ratios using a simple double pendulum with a mass ratio of 10000:1 as shown in Figure 5. In this case, optimization on the dual problem proceeds slowly, leading to large stretching. In contrast, primal-space optimization is relatively unaffected.

An equivalent result occurs in the contact scenario shown in Figure 8. Here the stack has a mass ratio of 4096:1 between the lower cylinder and the top one. For the primal solver we use contact parameters of $k_n = k_f = 10^8$ which is sufficient to stably support the stack. In contrast, dual-space optimization converges slowly for this case, leading to large interpenetrations.

7.2. Stiffness Ratio Tests

A simple test to illustrate the effect of stiffness ratios is shown in Figure 4. Here two point masses are connected by springs with stiffness coefficents that vary by a ratio of 10000:1. Although both springs are stiff enough to easily support the masses, when combined with a descent-based solver, the much stiffer lower spring

(a) $k_f = 10^2$ (b) $k_f = 10^3$ (c) $k_f = 10^4$ (d) Dual

Figure 10: ***Grasp Stability***. *We measure the effect of frictional stiffness on grasp stability. Here the Yumi robot picks up a cube, attempts to lift it to a height of 8cm, and remain stationary. Each image shows the final state of a grasp after 15s. We show the effect of varying friction stiffness with k_f increasing from left to right. Low stiffness results in visible slipping, but with high stiffness with implicit integration can be made nearly as stable as hard contact (dual) models over long periods of time.*

has the effect of slowing convergence for the top spring, resulting in significant stretching. Dual-space solvers do not suffer from any ill-conditioning in this case, showing the correct (unstretched) behavior.

An equivalent, but less obvious, stiffness ratio problem occurs in contacting scenarios where the normal and friction stiffness coefficients k_n and k_f differ by a large magnitude. In Figure 9 we see the effect of raising the contact stiffness while leaving the friction stiffness fixed. When combined with an iterative method, this has the effect of reducing friction convergence, leading to slip.

7.3. Rigid Piling

To investigate the performance of each method on large scale unstructured piling we simulate a granular material consisting of 256k rigid bodies as shown in Figure 1. The grains consist of spherical bodies with an average radius of 5mm and a mass of 5g. We use contact parameters of $k_n = k_f = 10^4$ and $\mu = 0.3$. A large cylindrical weight is dropped onto the pile creating a mass ratio of 80000:1. After 1.25s one of the walls is removed, allowing the grains to flow out. For primal methods we see that the grains support the weight easily, while dual optimization with the same iteration count shows significant compression.

A second example is illustrated in Figure 2. In this case, 512 bowls each represented by a triangle mesh with 1160 faces are dropped from a height. We use contact parameters of $k_n = k_f = 10^6$, and $\mu = 0.7$. This example is inspired by Xu & Barbic [XZB14], who simulated large plate stacks with a direct method. They used distance field based collision detection that generated 8.5k maximum contacts. Our triangle-based representation generates 393k contacts when settled (40x larger), however our parallel gradient-based solver still runs at real time rates and forms a stable pile. In this example we see similar behavior with both primal and dual based solvers. This is expected since there are no significant sources of ill-conditioning. Nevertheless, this example shows that the use of primal contact models and descent based optimization is practical as an alternative to iterative dual methods that may traditionally be used for such simulations.

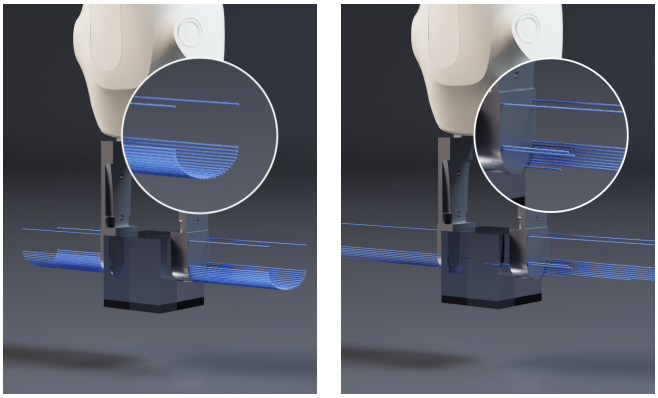

(a) (b)

Figure 11: ***Force Distributions***. *We visual contact normal forces in blue. The distribution of forces generated by a relaxed primal contact model are smooth (left). For hard contact models the problem is underdetermined, leading to a solution that depends on the ordering of contacts (right).*

7.4. Force Distributions

In real world scenarios, for example a tessellated cylinder resting on the ground, there are often many redundant contact constraints. This creates an underdetermined problem, with many possible contact force distributions that are all valid solutions. In this case, hard-contact solvers may produce an unpredictable distribution that is dependent on the ordering of constraints. In some applications uniform force distributions are desirable, for example, in sound synthesis Zheng et al. [ZJ11] used a secondary per-pair optimization to generate smooth contact forces. A benefit of the relaxed primal model presented here is that it generates evenly distributed forces without additional post-processing. An example of this is shown in Figure 11. Here the ABB Yumi robot grips a cube. The gripper is tessellated somewhat non-uniformly, but in a relaxed primal model of contact the system remains well-posed and leads to a smooth distribution of contact forces over the vertices.

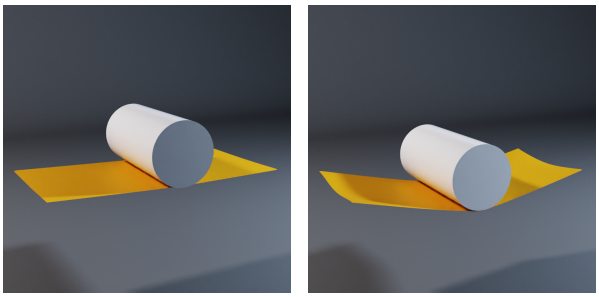

(a) Primal (b) Dual

Figure 12: ***Cloth Simulation***. *For an object suspended by inextensible cloth ($k = 10^{10}$) we find that primal methods (left) are able to achieve higher effective stiffness that dual (right) in an equivalent number of iterations.*

7.5. Cloth

To investigate the behavior of each method on deformable simulation, we suspend a piece of cloth modeled by 800 triangles and drop a rigid body onto it from a height, as shown in Figure 12. Surprisingly, the dual solution does not become stiffer after some elastic stiffness threshold value around $k = 10^8$. The same effect was observed by Soler et al. [SMSH18] in the context of Cosserat rods. We found this effect was consistent even in the absence of contact, and believe this behavior can be explained by the use of an approximate solution to the primal optimization subproblem in the dual update. In this case a hybrid method like the one used by Narain et al. [NSO12] for cloth strain-limiting may perform better.

7.6. Grasp Stability

Without some additional history-based contact tracking, relaxed models of friction do not generate frictional forces at zero-velocity. This means some allowed slip is expected. We measure the error induced by the this approximation on a robotic manipulation task shown in Figure 10. We found that for low values of k_f the robot was unable to hold the cube stationary. However, for high enough coefficients we found that primal contact was competitive with the dual baseline (Figure inset).

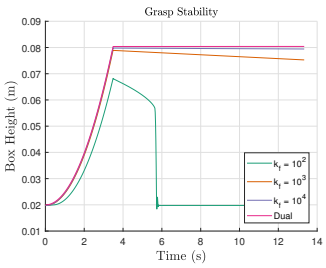

7.7. Differentiability

We show an example of trajectory optimization in Figure 13. Given an initial trajectory that involves impacts with two surfaces, the goal is to find a starting impulse such that a bouncing ball hits a target at $t = 0.5$s. We use a discrete adjoint method to perform reverse mode differentiation through the primal contact solver and optimize the loss function using an L-BFGS optimizer [LN89]. Primal formulations of contact are well-suited to differentiability for two reasons. First, the contact forces may be smoothed to provide C^2 continuity required for some optimization methods. Second, when performing reverse mode differentiation the state of the system must be saved at each forward step to compute the correct gradients during the backwards pass. For primal contact the size of the system is fixed regardless of the number of contacts. In contrast, the dual system must store a varying, and potentially large amount of contact information at each forward step.

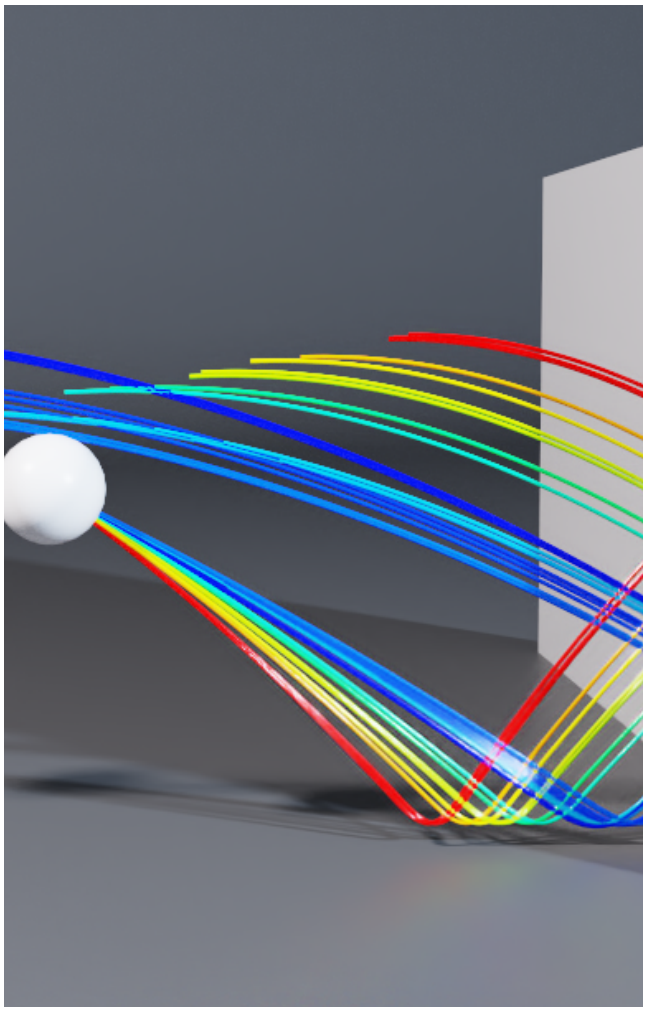

Figure 13: ***Differentiability***. *A trajectory optimization test using differentiable simulation to minimize the distance to a target through two contact events. Our primal contact model is well-suited to differentiability since it may be smoothed, and the system size remains fixed regardless of the number of contacts.*

8. Discussion and Limitations

The lack of hard constraints in the primal form would appear to be a major limitation, however, it is often possible to design a re-

Table 1: *Simulation statistics and performance numbers for the examples in this paper. The per-iteration work done by primal and dual descent methods is similar so we expect timings to be consistent between methods. We report the timings in milliseconds per-frame for both methods.*

Example	Steps	Iters.	Contacts	Primal	Dual
	#	#	# (Avg)	ms	ms
Cylinder Stack	2	20	189	0.9	0.9
Capsule Lean	2	20	11	0.5	0.4
Yumi Grasp	4	80	60	6.4	6.8
Granular Material	8	30	1510k	1396.8	1136.7
Bowl Pile	8	15	393k	16.6	18.1
House of Cards	4	100	1.2k	9.3	8.6

duced system where constrained degrees of freedom are removed completely, e.g.: for articulated rigid bodies [Fea14, LLK19]. Our derivation in terms of generalized velocities naturally supports these types of re-parameterizations. In our experience, the biggest limitation of primal solvers is the effect of stiffness ratios on convergence. Stiffness ratios may manifest themselves in unexpected ways, for example in the leaning capsule scene in Figure 9. While it is often sufficient to simply set the contact and friction stiffness to the same value, some situations may require more careful authoring.

Our method is designed to work with the descent-based optimization form of Projective Dynamics presented by Wang et al. [WY16] that does not require pre-factorized matrices. The extension to prefactorized methods is not obvious, and we leave this future work. An advantage of the primal form is that it does not require the inversion of the mass matrix $\mathbf{M}$. This means it is possible to use consistent mass matrices, which are able to produce more accurate results for FEM-based simulations [CLK*19]. Primal formulations also make it particularly easy to perform implicit integration of arbitrary force models. For example, materials with nonlinear constitutive equations, or activation models with complex dynamics such as muscle-tendon units. Our primal formulation is applicable to any nonlinear energy (with the caveat that it may not find a global optimum for nonconvex models), however the dual form requires finding a suitable variable splitting that is most easily performed for quadratic energies.

9. Conclusion and Future Work

We have presented a unified derivation and analysis of primal and dual formulations of implicit integration from a variational perspective. In addition, we have presented a novel primal contact model with a robust preconditioner that is easy to incorporate into existing solvers such as Projective Dynamics. Our contributions extend these frameworks to large scale rigid body and robotics simulations that may have otherwise been treated with a separate method.

Our focus is on iterative descent-based methods, however we expect some of the effects described here will change when used with other methods, e.g.: direct solvers. For future work we plan to explore techniques to address the stiffness ratio problem in primal formulations. We believe accelerated descent and nonlinear conjugate gradient methods are promising methods to improve convergence, while maintaining scalability.

10. Acknowledgements

The authors would like to thank Ignacio Llamas and the Omniverse team at NVIDIA for their help preparing the images and video in the paper. We also thank Gilles Daviet for providing a preprint of his related work [Dav20].

References

[ATK17] ANDREWS S., TEICHMANN M., KRY P. G.: Geometric stiffness for real-time constrained multibody dynamics. In *Computer Graphics Forum* (2017), vol. 36, Wiley Online Library, pp. 235–246. 2, 4

[BBB07] BATTY C., BERTAILS F., BRIDSON R.: A fast variational framework for accurate solid-fluid coupling. *ACM Trans. Graph. 26*, 3 (July 2007). 3

[BET14] BENDER J., ERLEBEN K., TRINKLE J.: Interactive simulation of rigid body dynamics in computer graphics. *Comput. Graph. Forum 33*, 1 (Feb. 2014), 246–270. 3

[BML*14] BOUAZIZ S., MARTIN S., LIU T., KAVAN L., PAULY M.: Projective dynamics: fusing constraint projections for fast simulation. *ACM Transactions on Graphics (TOG) 33*, 4 (2014), 154. 1, 2, 3

[BOFN18] BROWN G. E., OVERBY M., FOROOTANINIA Z., NARAIN R.: Accurate dissipative forces in optimization integrators. *ACM Transactions on Graphics (TOG) 37*, 6 (2018), 1–14. 3

[BV04] BOYD S. P., VANDENBERGHE L.: *Convex optimization*. Cambridge university press, 2004. 4

[BW98] BARAFF D., WITKIN A.: Large steps in cloth simulation. In *Proceedings of the 25th annual conference on Computer graphics and interactive techniques* (1998), ACM, pp. 43–54. 2

[CBFAB97] CHARBONNIER P., BLANC-FÉRAUD L., AUBERT G., BARLAUD M.: Deterministic edge-preserving regularization in computed imaging. *IEEE Transactions on image processing 6*, 2 (1997), 298–311. 8

[CLK*19] CHEN Y. J., LEVIN D. I., KAUFMANN D., ASCHER U., PAI D. K.: Eigenfit for consistent elastodynamic simulation across mesh resolution. In *Proceedings of the 18th annual ACM SIGGRAPH/Eurographics Symposium on Computer Animation* (2019), pp. 1–13. 11

[Dav20] DAVIET G.: Simple and scalable frictional contacts for thin nodal objects. *ACM Transactions on Graphics (TOG) 39*, 4 (2020). 3, 5, 11

[DBDB11] DAVIET G., BERTAILS-DESCOUBES F., BOISSIEUX L.: A hybrid iterative solver for robustly capturing coulomb friction in hair dynamics. In *ACM Transactions on Graphics (TOG)* (2011), vol. 30, ACM, p. 139. 3

[Dru07] DRUMWRIGHT E.: A fast and stable penalty method for rigid body simulation. *IEEE transactions on visualization and computer graphics 14*, 1 (2007), 231–240. 2

[EMP*03] EBERT D. S., MUSGRAVE F. K., PEACHEY D., PERLIN K., WORLEY S.: *Texturing & modeling: a procedural approach*. Morgan Kaufmann, 2003. 8

[Erl13] ERLEBEN K.: Numerical methods for linear complementarity problems in physics-based animation. In *ACM SIGGRAPH 2013 Courses* (2013), ACM, p. 8. 3

[Erl17] ERLEBEN K.: Rigid body contact problems using proximal operators. In *Proceedings of the ACM Symposium on Computer Animation* (2017), p. 13. 7

[Fea14] FEATHERSTONE R.: *Rigid body dynamics algorithms*. Springer, 2014. 11

[GHF*07] GOLDENTHAL R., HARMON D., FATTAL R., BERCOVIER M., GRINSPUN E.: Efficient simulation of inextensible cloth. In *ACM Transactions on Graphics (TOG)* (2007), vol. 26, ACM, p. 49. 2, 5

[GSS*15] GAST T. F., SCHROEDER C., STOMAKHIN A., JIANG C., TERAN J. M.: Optimization integrator for large time steps. *IEEE transactions on visualization and computer graphics 21*, 10 (2015), 1103–1115. 2, 3

[Joh85] JOHNSON K. L.: *Contact Mechanics*. Cambridge University Press, 1985. 7

[KSJP08] KAUFMAN D. M., SUEDA S., JAMES D. L., PAI D. K.: Staggered projections for frictional contact in multibody systems. In *ACM Transactions on Graphics (TOG)* (2008), vol. 27, ACM, p. 164. 3, 7

[LBOK13] LIU T., BARGTEIL A. W., O'BRIEN J. F., KAVAN L.: Fast simulation of mass-spring systems. *ACM Transactions on Graphics (TOG) 32*, 6 (2013), 214. 2

[LFS*20] LI M., FERGUSON Z., SCHNEIDER T., LANGLOIS T., ZORIN D., PANOZZO D., JIANG C., KAUFMAN D. M.: Incremental potential contact: Intersection- and inversion-free large deformation dynamics. *ACM Transactions on Graphics 39*, 4 (2020). 3, 6

[LJBBD20] LY M., JOUVE J., BOISSIEUX L., BERTAILS-DESCOUBES F.: Projective Dynamics with Dry Frictional Contact. *ACM Transactions on Graphics 39*, 4 (2020), 1–8. 3

[LLK19] LI J., LIU T., KAVAN L.: Fast simulation of deformable characters with articulated skeletons in projective dynamics. In *Proceedings of the 18th annual ACM SIGGRAPH/Eurographics Symposium on Computer Animation* (2019), pp. 1–10. 11

[LN89] LIU D. C., NOCEDAL J.: On the limited memory bfgs method for large scale optimization. *Mathematical programming 45*, 1-3 (1989), 503–528. 10

[MHHR07] MÜLLER M., HEIDELBERGER B., HENNIX M., RATCLIFF J.: Position based dynamics. *J. Vis. Comun. Image Represent. 18*, 2 (Apr. 2007), 109–118. 2

[MKB*10] MARTIN S., KAUFMANN P., BOTSCH M., GRINSPUN E., GROSS M.: Unified simulation of elastic rods, shells, and solids. In *ACM SIGGRAPH 2010 Papers* (New York, NY, USA, 2010), SIGGRAPH '10, ACM, pp. 39:1–39:10. 2

[MMC16] MACKLIN M., MÜLLER M., CHENTANEZ N.: Xpbd: position-based simulation of compliant constrained dynamics. In *Proceedings of the 9th International Conference on Motion in Games* (2016), ACM, pp. 49–54. 1, 2, 5

[MMFN14] MAZHAR H., MELANZ D., FERRIS M., NEGRUT D.: *An Analysis of Several Methods for Handling Hard-Sphere Frictional Contact in Rigid Multibody Dynamics*. Tech. Rep. TR-2014-11, Simulation-Based Engineering Laboratory, University of Wisconsin-Madison., 09 2014. 3

[MO96] MARHEFKA D. W., ORIN D. E.: Simulation of contact using a nonlinear damping model. In *Proceedings of IEEE international conference on robotics and automation* (1996), vol. 2, IEEE, pp. 1662–1668. 2

[NE15] NIEBE S., ERLEBEN K.: Numerical methods for linear complementarity problems in physics-based animation. *Synthesis Lectures on Computer Graphics and Animation 7*, 1 (2015), 1–159. 3

[NSO12] NARAIN R., SAMII A., O'BRIEN J. F.: Adaptive anisotropic remeshing for cloth simulation. *ACM Transactions on Graphics 31*, 6 (Nov. 2012), 147:1–10. Proceedings of ACM SIGGRAPH Asia 2012, Singapore. 10

[OTSG09] OTADUY M. A., TAMSTORF R., STEINEMANN D., GROSS M.: Implicit contact handling for deformable objects. In *Computer Graphics Forum* (2009), vol. 28, Wiley Online Library, pp. 559–568. 3

[PO07] PANDOLFI A., ORTIZ M.: Finite element analysis of nonsmooth frictional contact. *Solid Mechanics and its Applications 3* (01 2007). 7

[PRM19] PAN Z., REN B., MANOCHA D.: Gpu-based contact-aware trajectory optimization using a smooth force model. In *Proceedings of the 18th Annual ACM SIGGRAPH/Eurographics Symposium on Computer Animation* (New York, NY, USA, 2019), SCA '19, Association for Computing Machinery. 2, 3

[SLM06] SERVIN M., LACOURSIERE C., MELIN N.: Interactive simulation of elastic deformable materials. In *Proceedings of SIGRAD Conference* (2006), pp. 22–32. 2

[SMSH18] SOLER C., MARTIN T., SORKINE-HORNUNG O.: Cosserat rods with projective dynamics. In *Computer Graphics Forum* (2018), vol. 37, Wiley Online Library, pp. 137–147. 10

[ST96] STEWART D. E., TRINKLE J. C.: An implicit time-stepping scheme for rigid body dynamics with inelastic collisions and coulomb friction. *International Journal for Numerical Methods in Engineering 39*, 15 (1996), 2673–2691. 3

[Sta09] STAM J.: Nucleus: Towards a unified dynamics solver for computer graphics. In *Computer-Aided Design and Computer Graphics, 2009. CAD/Graphics' 09. 11th IEEE International Conference on* (2009), IEEE, pp. 1–11. 2

[Ste00] STEWART D. E.: Rigid-body dynamics with friction and impact. *SIAM review 42*, 1 (2000), 3–39. 7

[TBV12] TONGE R., BENEVOLENSKI F., VOROSHILOV A.: Mass splitting for jitter-free parallel rigid body simulation. *ACM Trans. Graph. 31*, 4 (July 2012), 105:1–105:8. 3, 8

[TET12] TODOROV E., EREZ T., TASSA Y.: Mujoco: A physics engine for model-based control. In *2012 IEEE/RSJ International Conference on Intelligent Robots and Systems* (2012), IEEE, pp. 5026–5033. 2

[TMOT12] TANG M., MANOCHA D., OTADUY M. A., TONG R.: Continuous penalty forces. *ACM Trans. Graph. 31*, 4 (2012), 107:1–107:9. 2

[TNGF15] TOURNIER M., NESME M., GILLES B., FAURE F.: Stable constrained dynamics. *ACM Transactions on Graphics (TOG) 34*, 4 (2015), 132. 2, 4, 7

[Tod14] TODOROV E.: Convex and analytically-invertible dynamics with contacts and constraints: Theory and implementation in mujoco. In *2014 IEEE International Conference on Robotics and Automation (ICRA)* (2014), IEEE, pp. 6054–6061. 2

[TWL*18] TANG M., WANG T., LIU Z., TONG R., MANOCHA D.: I-cloth: Incremental collision handling for gpu-based interactive cloth simulation. *ACM Transactions on Graphics (TOG) 37*, 6 (2018), 1–10. 3

[VJ19] VERSCHOOR M., JALBA A. C.: Efficient and accurate collision response for elastically deformable models. *ACM Trans. Graph. 38*, 2 (Mar. 2019). 3

[Wan15] WANG H.: A chebyshev semi-iterative approach for accelerating projective and position-based dynamics. *ACM Transactions on Graphics (TOG) 34*, 6 (2015), 246. 1, 2

[WY16] WANG H., YANG Y.: Descent methods for elastic body simulation on the gpu. *ACM Transactions on Graphics (TOG) 35*, 6 (2016), 212. 1, 2, 3, 4, 11

[XZB14] XU H., ZHAO Y., BARBIC J.: Implicit multibody penalty-baseddistributed contact. *IEEE transactions on visualization and computer graphics 20*, 9 (2014), 1266–1279. 2, 9

[YN06] YAMANE K., NAKAMURA Y.: Stable penalty-based model of frictional contacts. In *Proceedings 2006 IEEE International Conference on Robotics and Automation, 2006. ICRA 2006.* (2006), IEEE, pp. 1904–1909. 2

[ZJ11] ZHENG C., JAMES D. L.: Toward high-quality modal contact sound. *ACM Transactions on Graphics (Proceedings of SIGGRAPH 2011) 30*, 4 (Aug. 2011). 9